# EVLA Memo #182
# API Qualification Testing Results

*Keith Morris*
*September 14, 2014*

## 1 Background and Purpose

Phase I of the new API design called for co-locating the new instrument with the existing instrument. With this co-located geometry, both instruments should be measuring the same parcel of air over the same 10-minute interval allowing the derived saturation phase determined with the new and existing APIs to be compared directly.

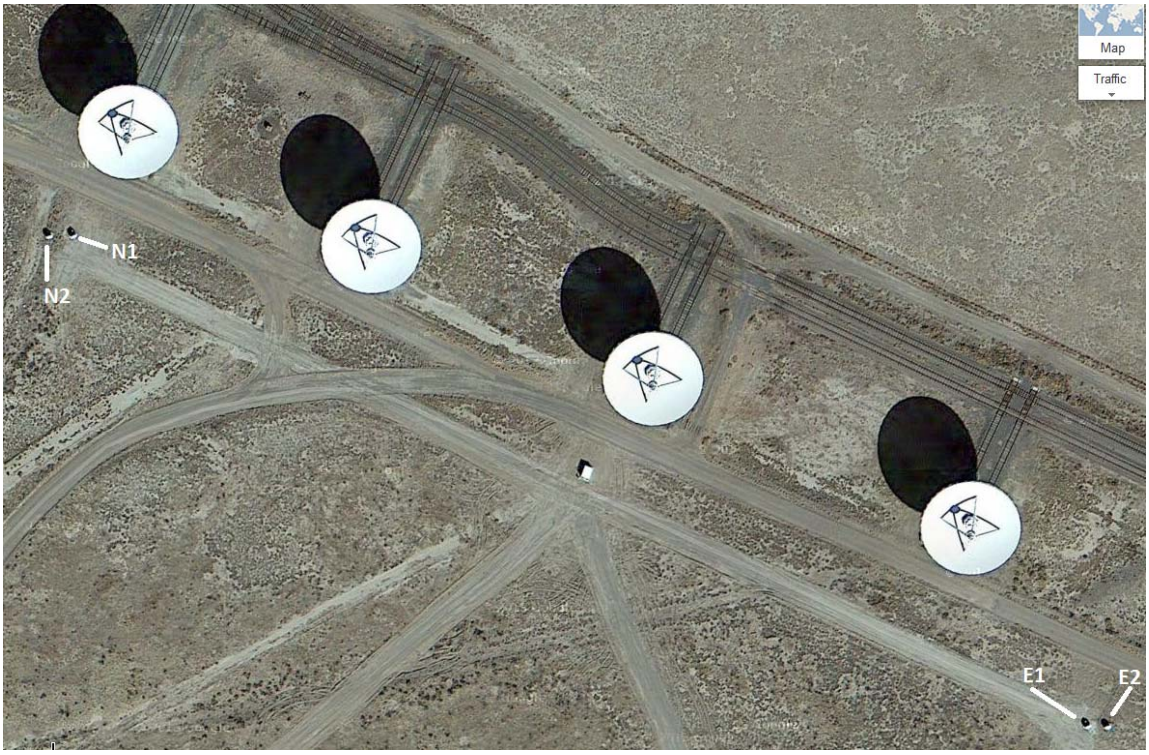


**Figure 1: API map, showing locations of new API antennas N1 and E1 and temporary installations N2 and E2, which are the sites of the original VLA API antennas**

## 2 Side-by-Side Qualification Tests

Before the new instrument can be accepted and the old instrument can be decommissioned, we must demonstrate that the new API meets its saturation phase measurement RMS requirement (0.4 degrees). Radford et al. [1996] outline a method for measuring the internal sensitivity, or instrumental noise floor of an API, by placing the receiving antennas as close as possible together. Doing this, they derived an electronic noise floor of $0.2^{o}$ over 60-second intervals for their instrument. Unfortunately, we cannot make a similar measurement given current constraints of where antennas can be located at the VLA site. Note that once the old API is

decommissioned, we can indeed make this measurement, but not before. The test will require that the old API antennas are integrated into the new API electronics.

Since we cannot make a measurement of the Radford noise floor RMS error until the old API is decommissioned, yet we cannot decommission the old API until we verify the performance of the new API, we are left in a dilemma. We have chosen to solve this dilemma by using a comparison of the saturation phase measurement of the new and old APIs as a proxy for the intrinsic measurement of the error of the new API. Since we think we know the electronic measurement error ($0.2^o$, since the instrument is similar to that described in Radford et al. [1996]) and the measurement error in saturation phase ($1.0^o$) for the old API, this comparison should be a good proxy for the saturation phase error of the new API.

The new instrument should produce the same value of saturation phase as the old instrument when they are measuring the same air parcel. Figure 2 shows five days of comparison data between the two API instruments from April 16 to April 21, 2014. It is encouraging to see that the red and blue curves are nearly identical, at least graphically.

We can further quantify the overall error between the two instruments by examining the difference of the saturation phase measurements between the two instruments over the five day period. Figure 3 shows the distribution of this error over the 714 points (~5 days) of data. A positive error indicates that the new API measured a higher value. The median difference is 0.2 degrees, indicating that the new instrument is still 0.2 degrees noisier than the old API.

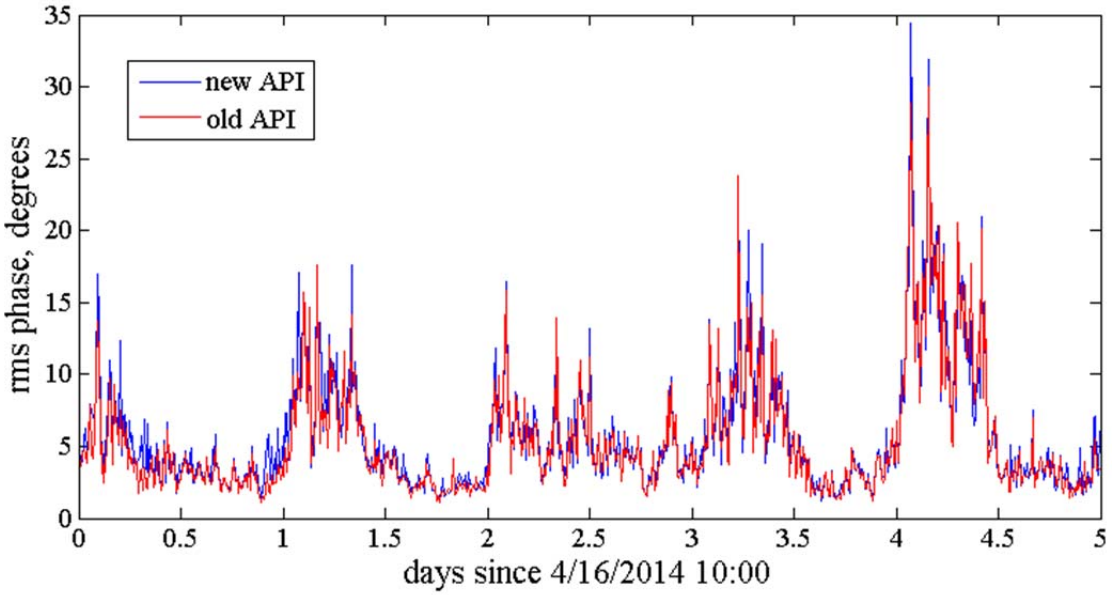


**Figure 2: Five days of API data for both instruments. New API is in red; old in blue.**

If these data were normally distributed, a true estimate of the difference between the two measurements could be obtained by measuring the mean, to estimate the center of the

distribution, and standard deviation (or RMS) to estimate its width. But the distribution is skewed, and outliers in the tails of the data will bias an estimate based on these traditional measures. The median is a more robust estimate than the mean of the center of such a distribution. To measure the width, we require a robust estimator that excludes outliers; the Median Average Deviation (MAD) is a sufficiently robust estimator, and from the MAD the RMS can be obtained by multiplying by 1.483 (Huber [1981]). Using the MAD robust estimator, the RMS of the distribution in Figure 3 is 1.9 degrees.

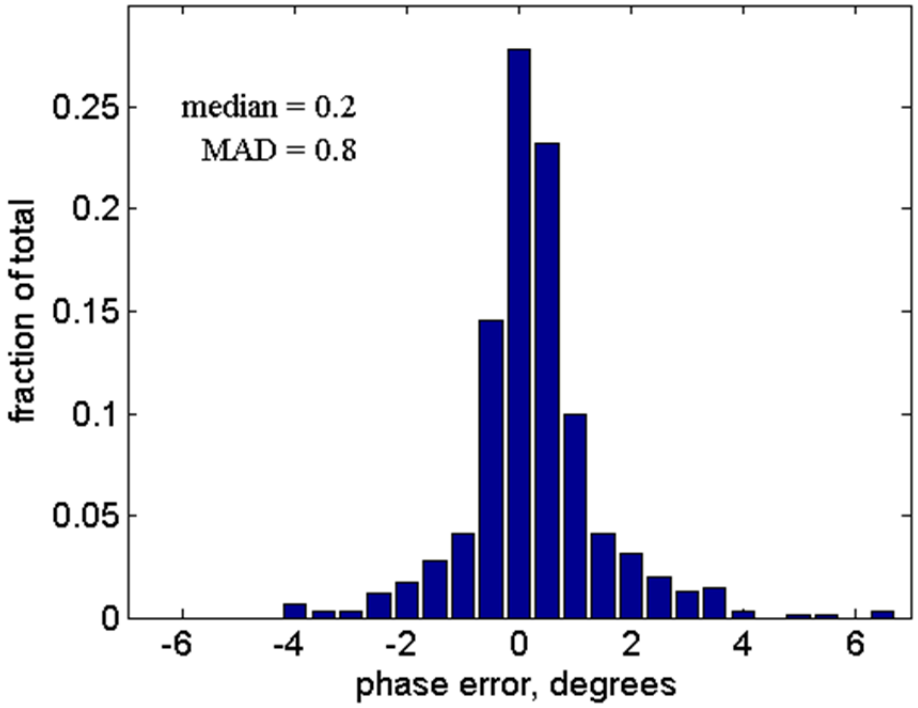


**Figure 3: Error distribution of difference in saturation phase measurement for 5 days of data for the two instruments.**

Even given the 0.2 degree bias in the new API saturation phase values, it is clear that the new API is performing at least as well as the old API, i.e., the RMS error between the two instruments is on the same order as the RMS uncertainty of the saturation phase measurement of the old API, which is taken to be ~1 degree. While this is not final proof that the new API is performing to its requirement, it is proof that it is performing as well as the old API, which, again, is a good proxy.

Figure 4 shows a histogram of the difference in the power-law exponents derived from data from the old and new APIs. The plot shows two peaks – one with a median difference of -0.03 and one with a median of -0.1; the standard deviations of the two overlapping distributions are 0.02 and 0.08, respectively. It is worth looking at the exponent histograms for each instrument, and to locate the source of the bimodality.

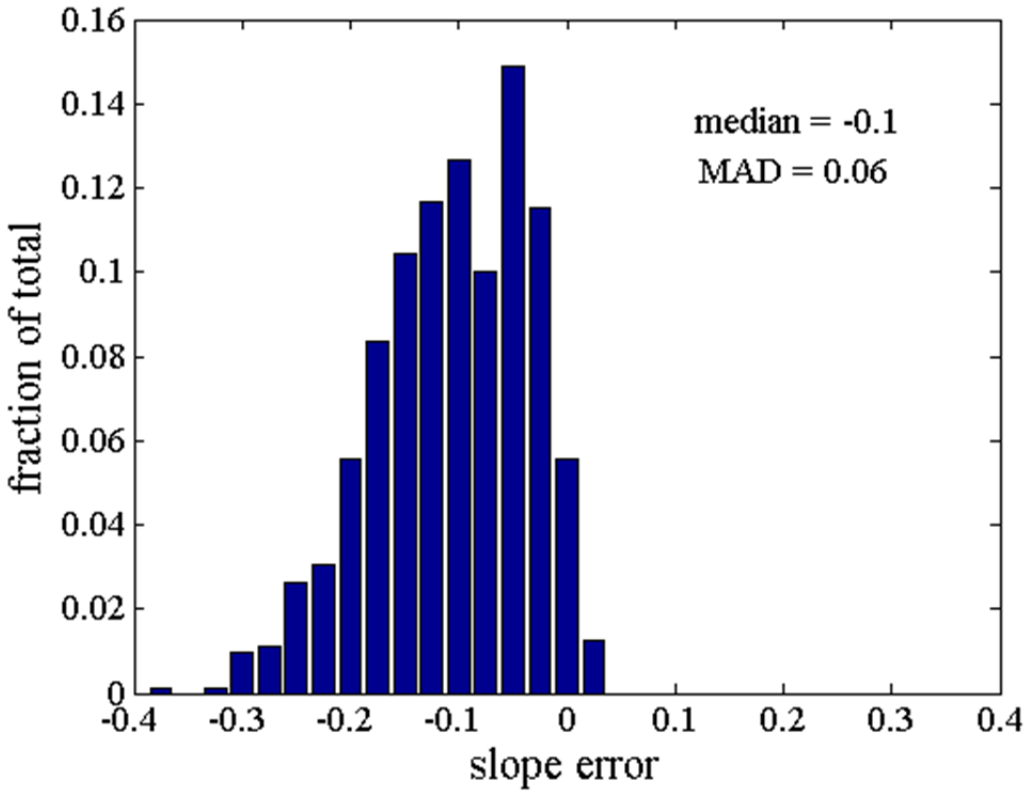


**Figure 4: Error distribution of difference in power law exponents, also called "slopes", for 5 days of data for the two instruments.**

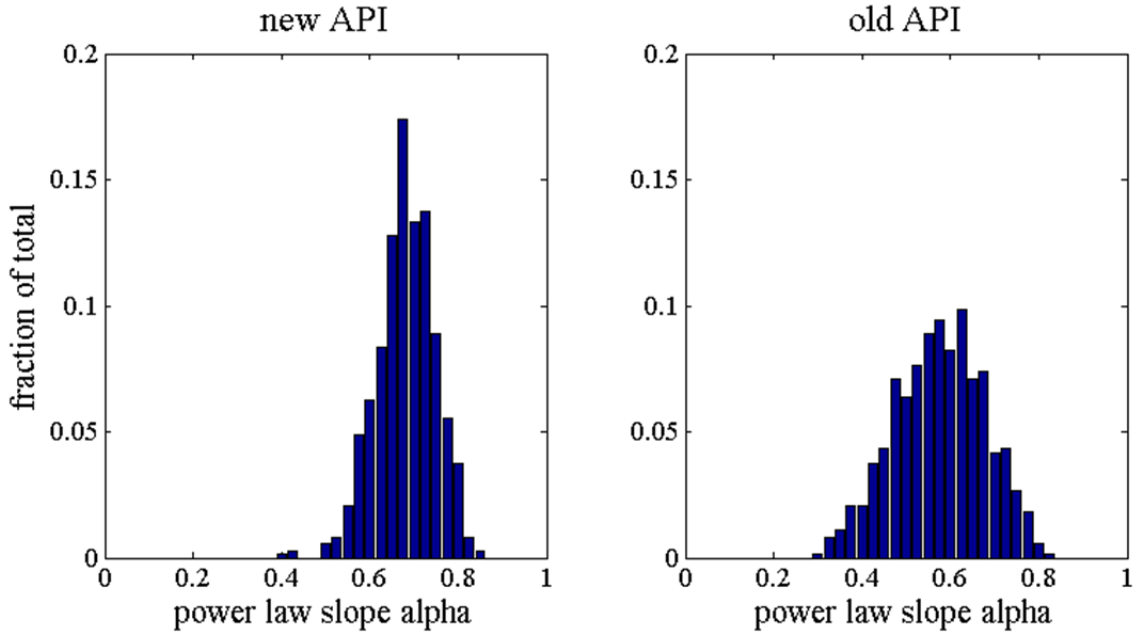


**Figure 5: Slope histograms for old API (left) and new API (right). The new API shows two overlapping slope distributions -- one at 0.63, indicating turbulence, and a second at 0.5, indicating instrumental noise.**

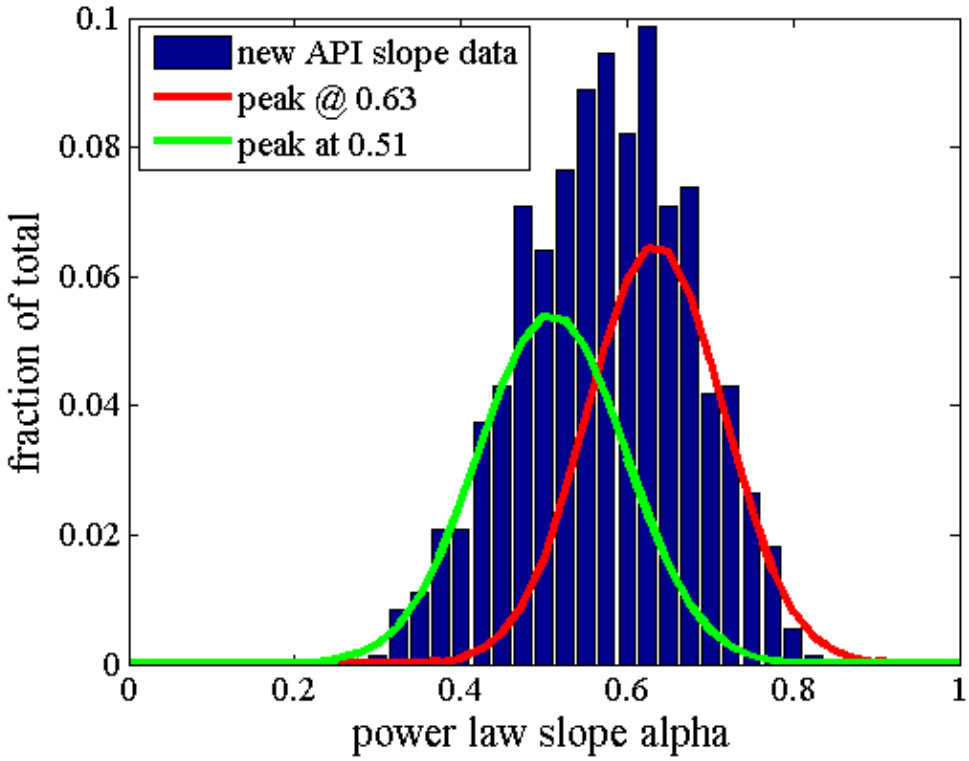


**Figure 6: Slope distribution for new API, April 16 - 21.**
**Bimodal distribution indicates the presence of a second random process.**

Figure 5 shows histograms of the slope measurements from each API over the 5-day period. The old API shows a tight distribution with a median value of 0.68, or nearly the theoretical value for isotropic 3D turbulence. The new API shows a wider asymmetrical distribution, with higher density along the lower (left) tail. This asymmetry requires explanation. As Figure 6 indicates, the excess spread in the new API slope distribution can be attributed to two overlapping distributions – one with a median value of 0.63, indicating turbulence, and one with a median of 0.5, indicating the presence of instrumental flicker noise. The distinct measurable second distribution peak gives us a valuable error-finding tool. This will aid in our efforts to bring the uncertainty of the new API measurement to less than half that of the old API.

## 3 Zero-Baseline Tests

On July 23, the original VLA API was officially decommissioned and powered off. At that point, its antennas were retrofitted with new API electronics, power supply and fiber optic connections. The fiber connections to these antenna pads are intended to be temporary only, and as such were not buried, as with the permanent API antenna installations.

The purpose of this temporary antenna configuration is to test the 4-element system while the effects of array geometry are minimized – the two pairs of antennas form baselines equivalent in length and orientation to each other, as in the side-by-side tests of old vs new API. Pending the completion of this test, the two antennas will be relocated to their final locations at the former ALMA Test Facility and near the VLA Visitor's RV Parking Area.

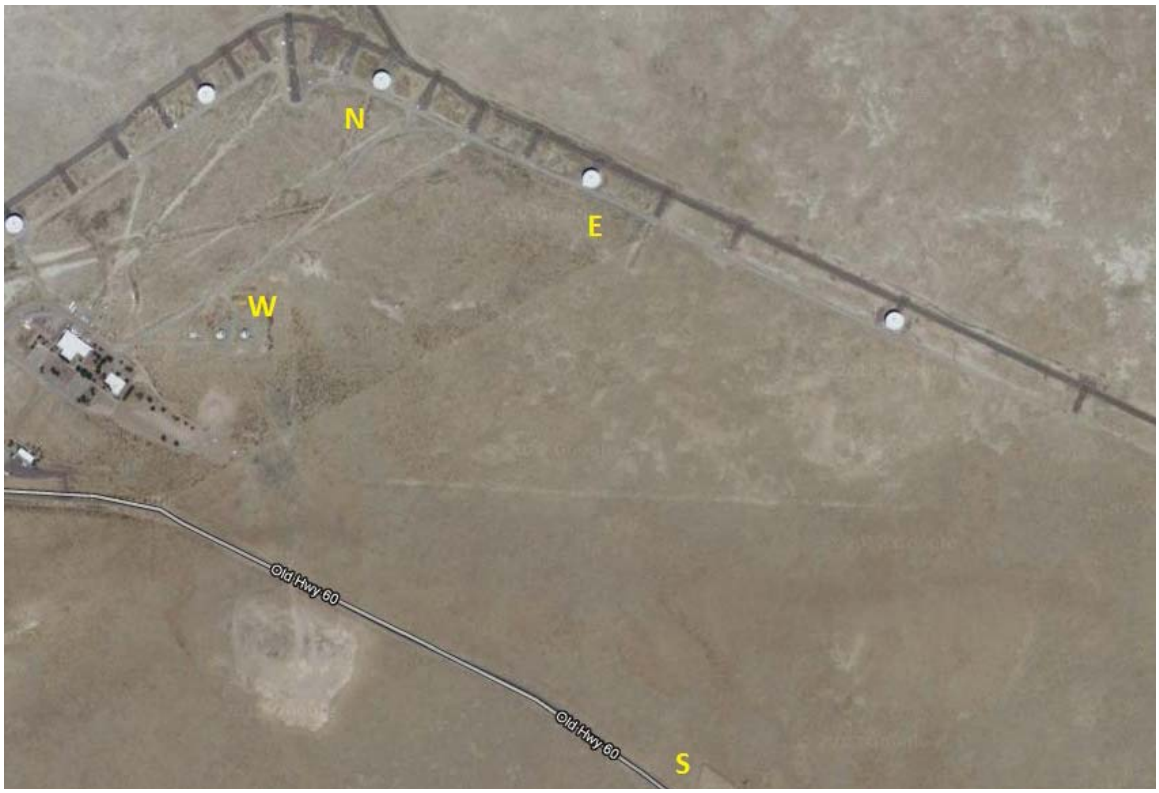


**Figure 7: Map of final API array geometry**

The four antennas are connected to the M360 API Data Acquisition module, which forms six cross-products whose phases and root phase structure functions are reported to the Monitor Data Archive. We will label the two permanent new API antennas "N1" and "E1" (later to be renamed simply "N" and "E") and the two temporary installations "N2" and "E2" (later to be moved and renamed to "W" and "S", respectively). Then the six measurement baselines are:

**Table 1: Phase measurement baseline definitions**

| Monitor Data Label | Antenna 1 | Antenna 2 |
|---|---|---|
| Phase0 | N1 | E1 |
| Phase1 | N1 | N2 |
| Phase2 | N1 | E2 |
| Phase3 | E1 | N2 |
| Phase4 | E1 | E2 |
| Phase5 | E2 | N2 |

The two highlighted rows in Table 1, phase1 and phase4, represent the two "zero-baseline" cases, where the antenna separation is less than 10 meters. Each zero-baseline pair comprises a standard production "New API" antenna (N1 or E1), and a modified temporary "New API" antenna (N2 or E2). The zero-baseline measurements are expected to be dominated by system

electronic noise and temperature instability, since the antenna separation is so small as to be considered a shared atmospheric path; however there is some weak visual evidence for turbulence measurement on this length scale.

The overall RMS phase for these pairs is lower than for the four 300m baseline pairs, and in principle the zero-baseline pairs would give the lower limit for the measurement, other things being equal. But other things were not equal, namely:

1. The 10MHz LO fiber receivers had not yet been updated on N2 and E2
2. The fiber for N2 and E2 were spliced out of the N1 and E1 splice boxes and the fibers are lying across the ground. Each had approximately 4 meters of fiber optic cable in independent thermal environments
3. N2 and E2 use a different manufacturer's LNB than N1 and E1.

Of these, (1) is in the author's opinion the most significant, and the other considerations are listed in decreasing order of assumed significance.

Figure 8 shows a histogram of the entire five nights' worth of measurements for RMS_PHASE1, which measures the N1-N2 baseline. This distribution shows a minimum value of 0.6 degrees, mode of 1.3 degrees, and a median value of 1.5 degrees. The lower limit to this value is assumed to be set by the electronics system noise floor. That is certainly one component of the sensitivity limit. And given (1) in the list above, a component that is expected to be reduced shortly.

The structure function slopes of the zero-baseline pairs are in fact dominated by noise, up to lags of about 10 seconds. Beyond ten seconds, the atmospheric structure emerges and takes on a slope closer to the canonical 0.67. But since the fitting algorithm performs a single linear fit to the non-saturation region of the structure function, the multiple slopes are not evident in the slope plots of Section 5. Figure 9 shows a typical, well-behaved phase structure function (Phase0), and Figure 10 shows the structure function for one of the zero-baseline pairs, Phase1.

## 4 Summary of Error Statistics

For each night of data, we compare the RMS phase measured on each of the six baselines to each other measurement baseline. Since Phase1 and Phase4 are measuring such small atmospheric cross-sections compared to the others, we do not expect the RMS phase on these baselines to correspond to the phase measured on the 300m baselines, and the resulting errors appear quite large; but these large errors are artificial and arbitrary, and do not represent a true state of the system. In the raw statistics tables of Section 5, cells that contain measurements involving these baselines are highlighted in grey.

Excluding errors involving Phase1 and Phase4, there are six valid error measures. The median errors are listed in Table 2 and the median absolute deviations of the error distributions are listed in Table 3. Each error is the median and MAD of the point-by-point difference of each pair of

ten-hour time series of synchronized RMS phase measurements. These data are shown graphically in Figure 11 and Figure 12 respectively.

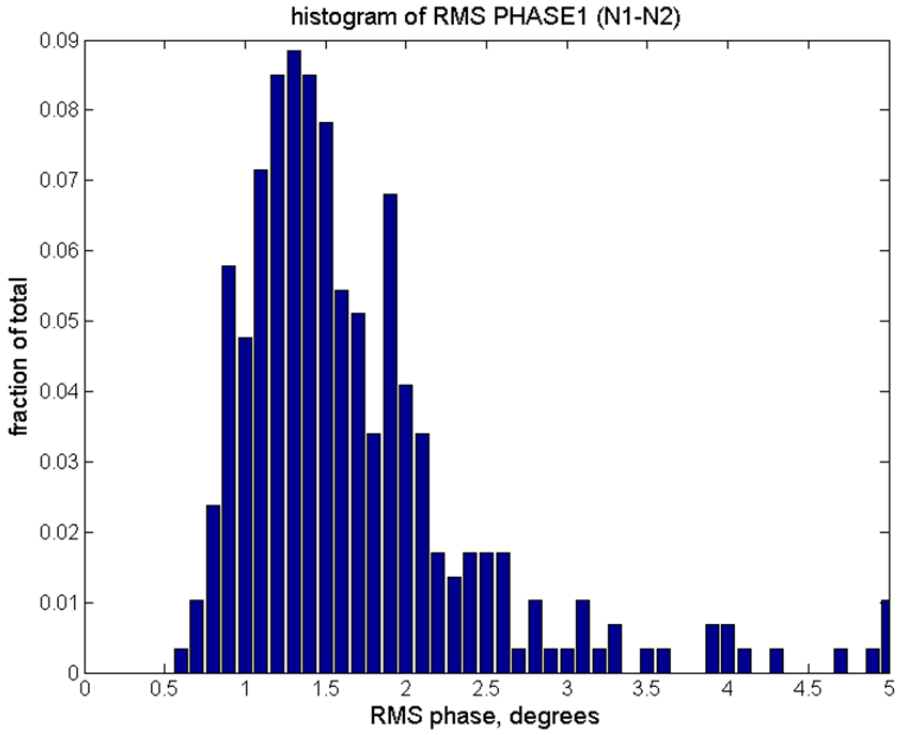


**Figure 8: Histogram of RMS_PHASE1 values for the five nights.**

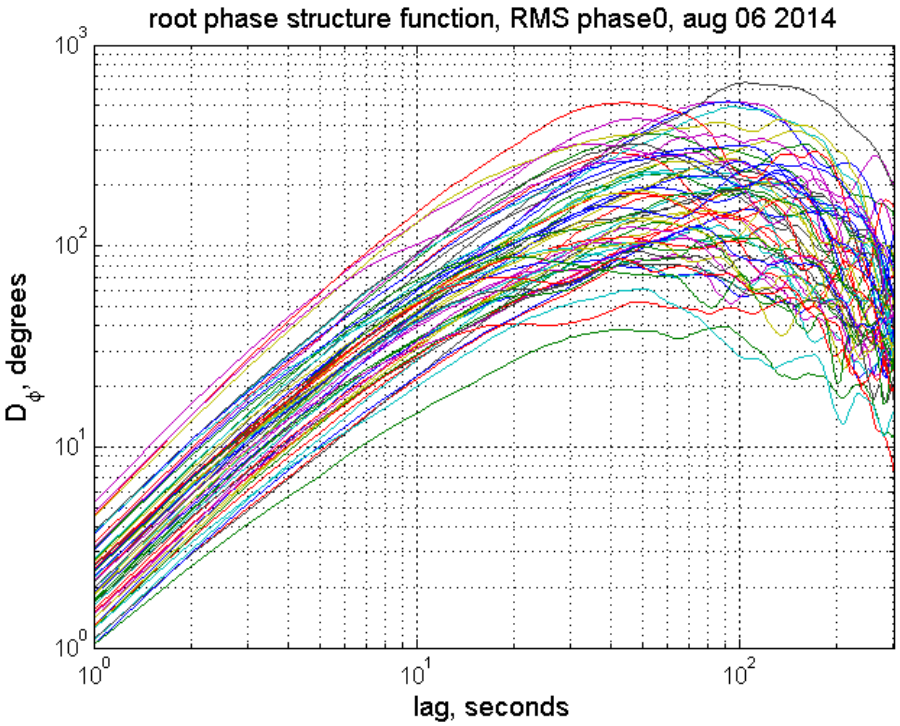


**Figure 9: Root phase structure function for Phase0, showing canonical 0.67 slope in the power-law region**

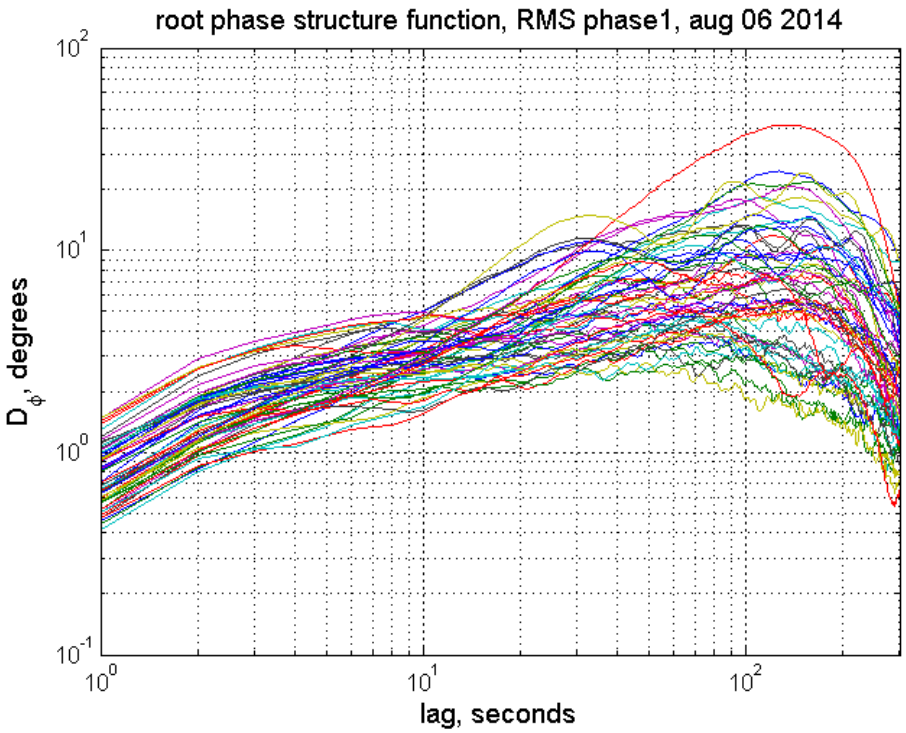


**Figure 10: Root phase structure function for Phase1, showing multiple power-law slopes**

**Table 2: Median RMS phase error across six baseline pairs for five ten-hour periods.**

| | Median Error, degrees | | | | |
|---|---|---|---|---|---|
| | August 06 | August 07 | August 08 | August 09 | August 10 |
| Phase0-Phase2 | -0.3 | -0.3 | -0.7 | -0.5 | -0.5 |
| Phase0-Phase3 | -0.1 | -0.1 | -0.2 | -0.2 | -0.3 |
| Phase0-Phase5 | -0.4 | -0.3 | -0.7 | -0.7 | -0.7 |
| Phase2-Phase3 | 0.2 | 0.2 | 0.3 | 0.2 | 0.4 |
| Phase2-Phase5 | -0.1 | -0.0 | -0.2 | -0.2 | -0.2 |
| Phase3-Phase5 | -0.3 | -0.2 | -0.6 | -0.5 | -0.3 |

**Table 3: Median Absolute Deviation (MAD) of the RMS phase error distributions from Table 2.**

| | MAD Error, degrees | | | | |
|---|---|---|---|---|---|
| | August 06 | August 07 | August 08 | August 09 | August 10 |
| Phase0-Phase2 | 0.6 | 0.6 | 1.1 | 2.6 | 1.0 |
| Phase0-Phase3 | 0.4 | 0.4 | 0.6 | 0.5 | 0.4 |
| Phase0-Phase5 | 0.7 | 0.7 | 1.3 | 1.5 | 1.0 |
| Phase2-Phase3 | 0.8 | 0.7 | 1.1 | 2.8 | 1.1 |
| Phase2-Phase5 | 0.4 | 0.3 | 0.7 | 1.8 | 0.5 |
| Phase3-Phase5 | 0.6 | 0.6 | 1.0 | 1.5 | 1.1 |

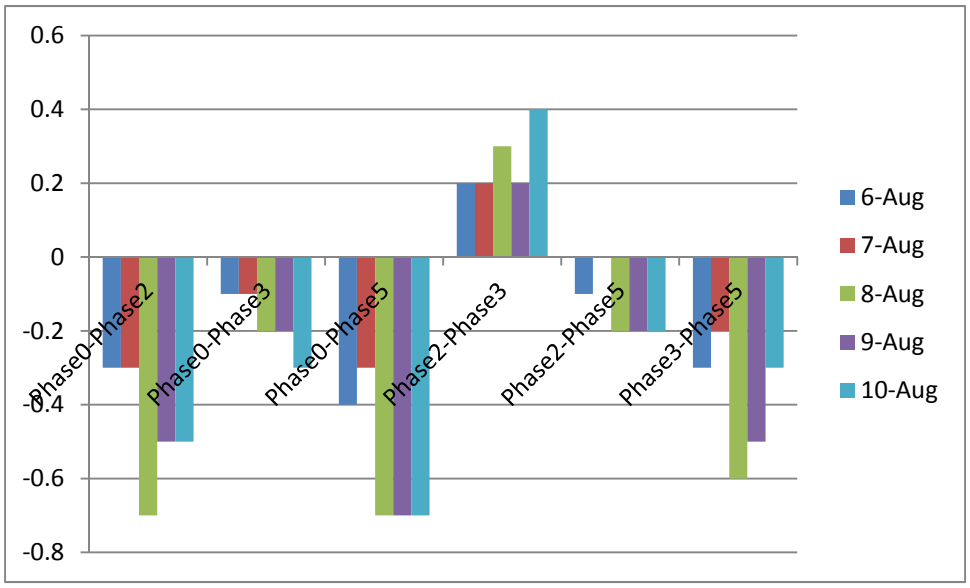


**Figure 11: Median pair-wise RMS phase difference for the five nights.**

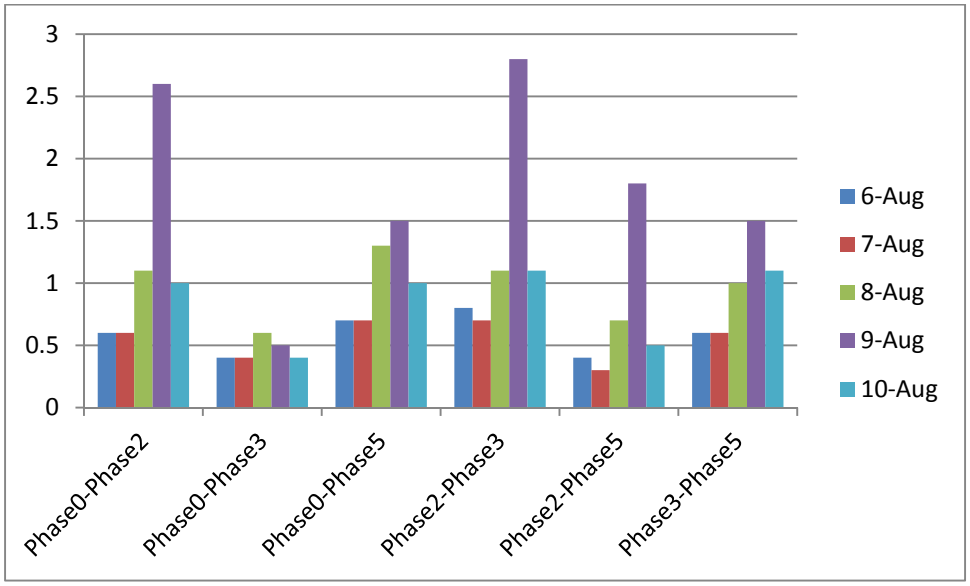


**Figure 12: MAD of the pair-wise RMS phase differences in chart form. Notice that August 09 was a particularly bad night for every pair of phase measurements.**

In general, we see that the pairs with the lowest median error are phase0-phase3 and phase2-phase5, two cases where a matched antenna pair is compared to a mixed permanent-temporary antenna pair. The pair with the highest median error is phase0-phase5. Intuitively this makes sense, since these two sets antennas are matched internal to each pair, electronically, and not to the members of the other pair. We encounter the maximum independence of error sources under

these conditions. We expect that the API measurement is sensitive enough to capture the differences in antenna electronic and optical configuration.

The pairs phase0-phase3 and phase2-phase5 (with the exception of August 09) generally also show the lowest MAD in the error distributions – in other words, they are measuring mostly (small) systematic, and not random, phase errors.

## 5 Raw Error Statistics

The RMS phase and structure function slopes for each of the six baselines are shown in Figure 17. Table 4 lists the median error and median absolute deviation (MAD) for each pair of phases. The grey shaded cells in the tables are all difference to the two zero-baseline pairs, which are in principle measuring only system electronic noise, and cannot be construed as atmospheric measurements.

The significance of the negative sign in the median errors is that phase0 (N1-E1) in general has a lower RMS phase value than phase2 (N1-E2), phase3 (E1-N2), or phase5 (N2-E2). MAD error is always positive.

Error histograms for the two lowest-error pairs – phase0-phase3 and phase2-phase5 – and the highest-error pair – phase0-phase5 – are included for the five nights of the test. For comparison's sake, **Error! Reference source not found.** shows the corresponding error histogram for the old API-vs-new API test from five days in March 2014. The best of the permanent-vs-temporary antenna phase errors shows the same (0.2 degree) systematic error as the old-vs-new API tests from March 2013, and a lower (0.5 degree) random error.

**Table 4: Median (above) and MAD (below) errors in RMS phase for the six API baselines for the night of August 7, 2014.**

| Median error | Phase1 (N1-N2) | Phase2 (N1-E2) | Phase3 (E1-N2) | Phase4 (E1-E2) | Phase5 (N2-E2) |
|---|---|---|---|---|---|
| Phase0 (N1-E1) | 5.5 | -0.3 | -0.1 | 4.6 | -0.4 |
| Phase1 (N1-N2) | - | -6.0 | -5.8 | -0.7 | -6.1 |
| Phase2 (N1-E2) | | - | 0.2 | 5.0 | -0.1 |
| Phase3(E1-N2) | | | - | 4.6 | -0.3 |
| Phase4 (E1-E2) | | | | - | -5.0 |

| MAD error | Phase1 (N1-N2) | Phase2 (N1-E2) | Phase3 (E1-N2) | Phase4 (E1-E2) | Phase5 (N2-E2) |
|---|---|---|---|---|---|
| Phase0 (N1-E1) | 1.9 | 0.6 | 0.4 | 2.0 | 0.7 |
| Phase1 (N1-N2) | - | 1.8 | 1.9 | 0.7 | 1.8 |
| Phase2 (N1-E2) | | - | 0.8 | 1.8 | 0.4 |
| Phase3(E1-N2) | | | - | 2.1 | 0.6 |
| Phase4 (E1-E2) | | | | - | 1.9 |

**Table 5: Median (above) and MAD (below) errors in RMS phase for the six API baselines for the night of August 7, 2014.**

| Median error | Phase1 (N1-N2) | Phase2 (N1-E2) | Phase3 (E1-N2) | Phase4 (E1-E2) | Phase5 (N2-E2) |
|---|---|---|---|---|---|
| Phase0 (N1-E1) | 5.6 | -0.3 | -0.1 | 4.8 | -0.3 |
| Phase1 (N1-N2) | - | -6.0 | -6.1 | -0.5 | -5.9 |
| Phase2 (N1-E2) | | - | 0.2 | 4.8 | -0.0 |
| Phase3(E1-N2) | | | - | 5.3 | -0.2 |
| Phase4 (E1-E2) | | | | - | -5.1 |

| MAD error | Phase1 (N1-N2) | Phase2 (N1-E2) | Phase3 (E1-N2) | Phase4 (E1-E2) | Phase5 (N2-E2) |
|---|---|---|---|---|---|
| Phase0 (N1-E1) | 2.5 | 0.6 | 0.4 | 2.8 | 0.7 |
| Phase1 (N1-N2) | - | 2.4 | 2.4 | 1.1 | 2.3 |
| Phase2 (N1-E2) | | - | 0.7 | 2.7 | 0.3 |
| Phase3(E1-N2) | | | - | 2.7 | 0.6 |
| Phase4 (E1-E2) | | | | - | 2.6 |

**Table 6: Median (above) and MAD (below) errors in RMS phase for the six API baselines for the night of August 8, 2014.**

| Median error | Phase1 (N1-N2) | Phase2 (N1-E2) | Phase3 (E1-N2) | Phase4 (E1-E2) | Phase5 (N2-E2) |
|---|---|---|---|---|---|
| Phase0 (N1-E1) | 2.5 | -0.7 | -0.2 | 1.8 | -0.7 |
| Phase1 (N1-N2) | | -3.6 | -3.0 | -1.0 | -3.9 |
| Phase2 (N1-E2) | | | 0.3 | 2.3 | -0.2 |
| Phase3(E1-N2) | | | | 1.9 | -0.6 |
| Phase4 (E1-E2) | | | | | -2.7 |

| MAD error | Phase1 (N1-N2) | Phase2 (N1-E2) | Phase3 (E1-N2) | Phase4 (E1-E2) | Phase5 (N2-E2) |
|---|---|---|---|---|---|
| Phase0 (N1-E1) | 1.7 | 1.1 | 0.6 | 2.0 | 1.3 |
| Phase1 (N1-N2) | | 1.7 | 1.5 | 1.2 | 1.7 |
| Phase2 (N1-E2) | | | 1.1 | 1.4 | 0.7 |
| Phase3(E1-N2) | | | | 1.8 | 1.0 |
| Phase4 (E1-E2) | | | | | 1.5 |

**Table 7: Median (above) and MAD (below) errors in RMS phase for the six API baselines for the night of August 9, 2014.**

| Median error | Phase1 (N1-N2) | Phase2 (N1-E2) | Phase3 (E1-N2) | Phase4 (E1-E2) | Phase5 (N2-E2) |
|---|---|---|---|---|---|
| Phase0 (N1-E1) | 3.5 | -0.5 | -0.2 | 2.5 | -0.7 |
| Phase1 (N1-N2) | | -4.5 | -3.6 | -0.8 | -4.6 |
| Phase2 (N1-E2) | | | 0.2 | 3.4 | -0.2 |
| Phase3(E1-N2) | | | | 2.8 | -0.5 |
| Phase4 (E1-E2) | | | | | -3.3 |

| MAD error | Phase1 (N1-N2) | Phase2 (N1-E2) | Phase3 (E1-N2) | Phase4 (E1-E2) | Phase5 (N2-E2) |
|---|---|---|---|---|---|
| Phase0 (N1-E1) | 1.6 | 2.6 | 0.5 | 3.7 | 1.5 |
| Phase1 (N1-N2) | | 3.0 | 1.5 | 3.1 | 1.8 |
| Phase2 (N1-E2) | | | 2.8 | 3.5 | 1.8 |
| Phase3(E1-N2) | | | | 3.8 | 1.5 |
| Phase4 (E1-E2) | | | | | 2.8 |

**Table 8: Median (above) and MAD (below) errors in RMS phase for the six API baselines for the night of August 10, 2014.**

| Median error | Phase1 (N1-N2) | Phase2 (N1-E2) | Phase3 (E1-N2) | Phase4 (E1-E2) | Phase5 (N2-E2) |
|---|---|---|---|---|---|
| Phase0 (N1-E1) | 2.9 | -0. 5 | -0.3 | 1.9 | -0.7 |
| Phase1 (N1-N2) | | -4.0 | -3.1 | -0.8 | -3.9 |
| Phase2 (N1-E2) | | | 0.4 | 2.7 | -0.2 |
| Phase3(E1-N2) | | | | 2.3 | -0.3 |
| Phase4 (E1-E2) | | | | | -2.8 |

| MAD error | Phase1 (N1-N2) | Phase2 (N1-E2) | Phase3 (E1-N2) | Phase4 (E1-E2) | Phase5 (N2-E2) |
|---|---|---|---|---|---|
| Phase0 (N1-E1) | 1.7 | 1.0 | 0.4 | 1.9 | 1.0 |
| Phase1 (N1-N2) | | 2.0 | 1.6 | 1.2 | 2.0 |
| Phase2 (N1-E2) | | | 1.1 | 1.7 | 0.5 |
| Phase3(E1-N2) | | | | 1.9 | 1.1 |
| Phase4 (E1-E2) | | | | | 1.8 |

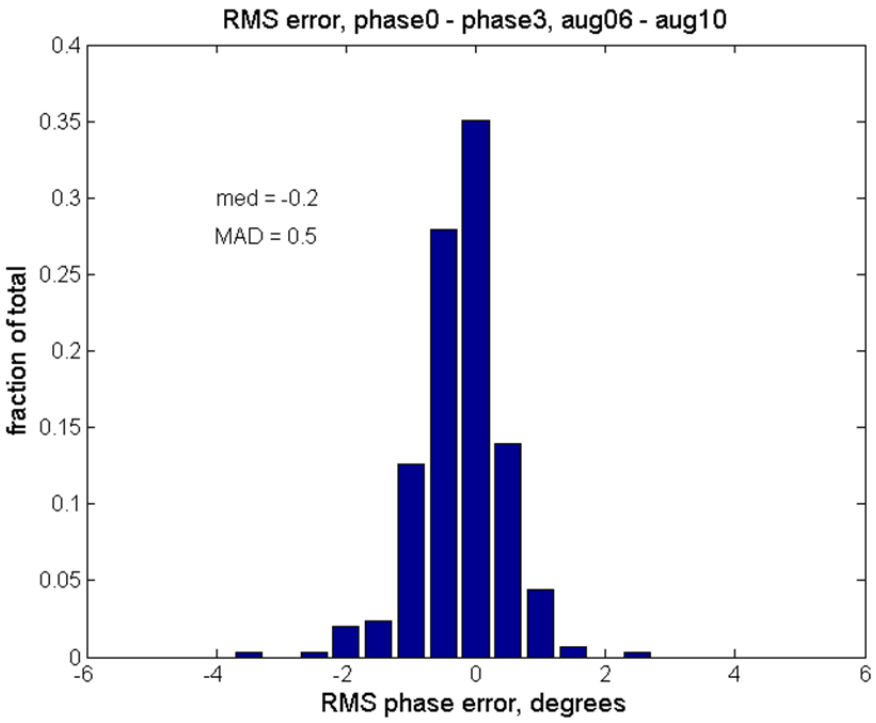


**Figure 13: Error histogram for phase0 - phase3, the pair with the lowest median error**

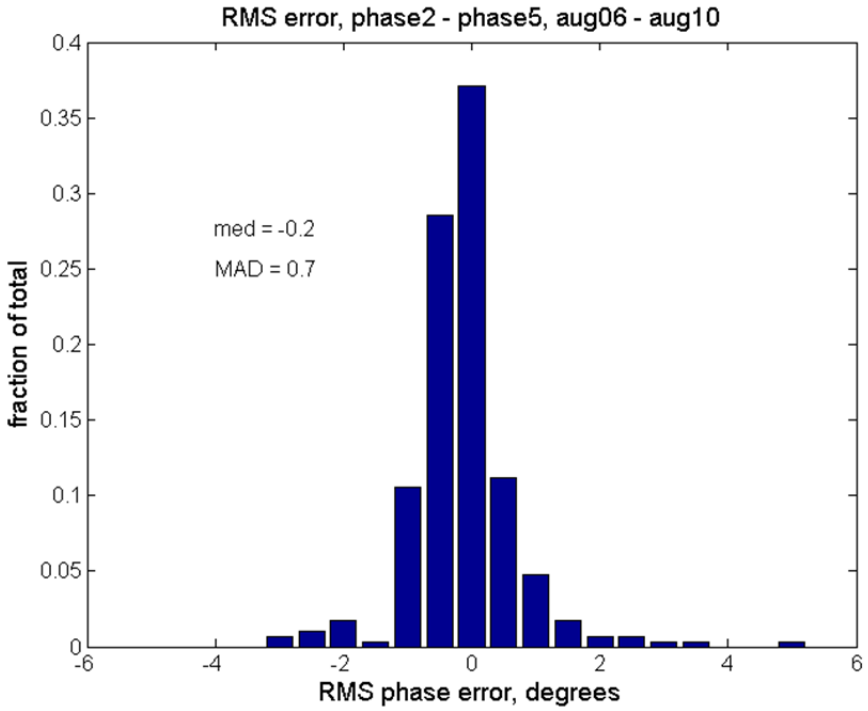


**Figure 14: Error histogram for phase2 - phase5,**
**the pair with a comparably low median error to phase0 - phase3.**

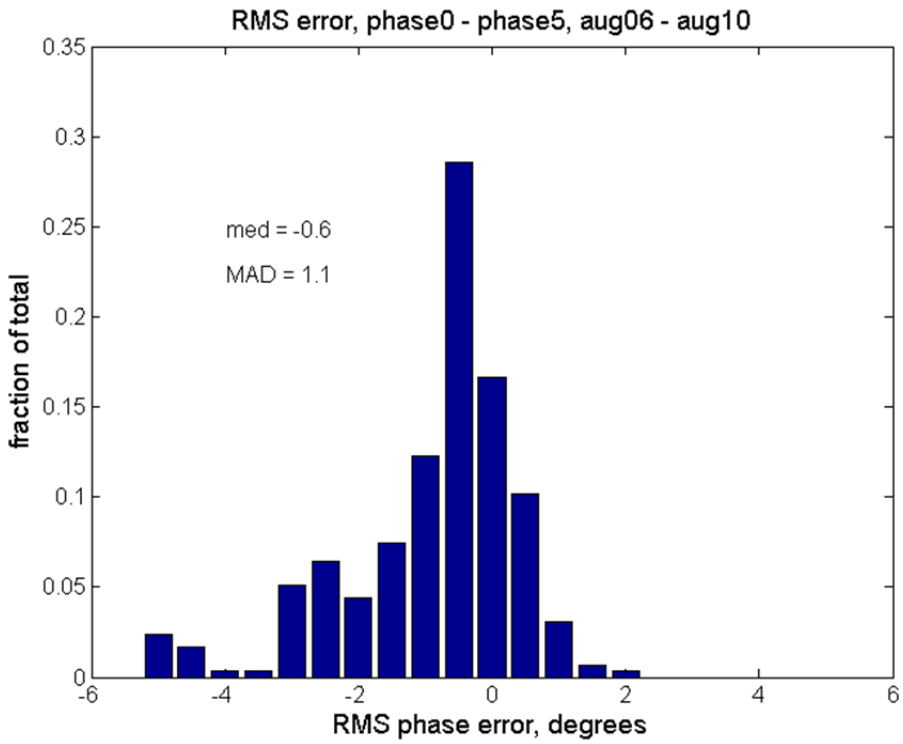


**Figure 15: Error histogram for phase0 - phase5, the measurement with the highest median error**

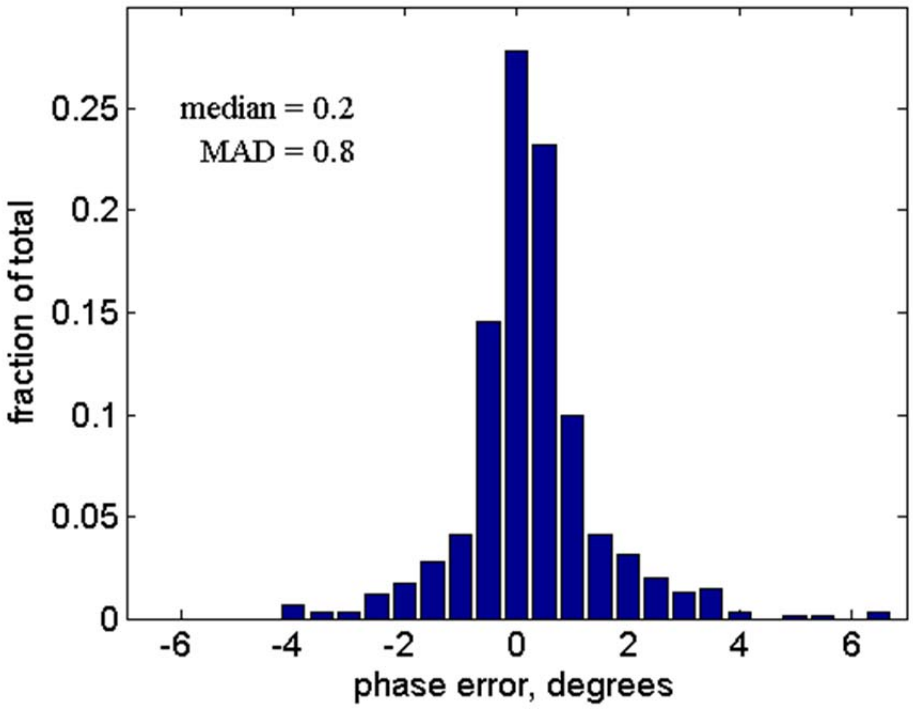


**Figure 16: Error distribution, new versus old API, April 6 - April 10**

## 6 Plots of RMS Phase and Power Law Slope

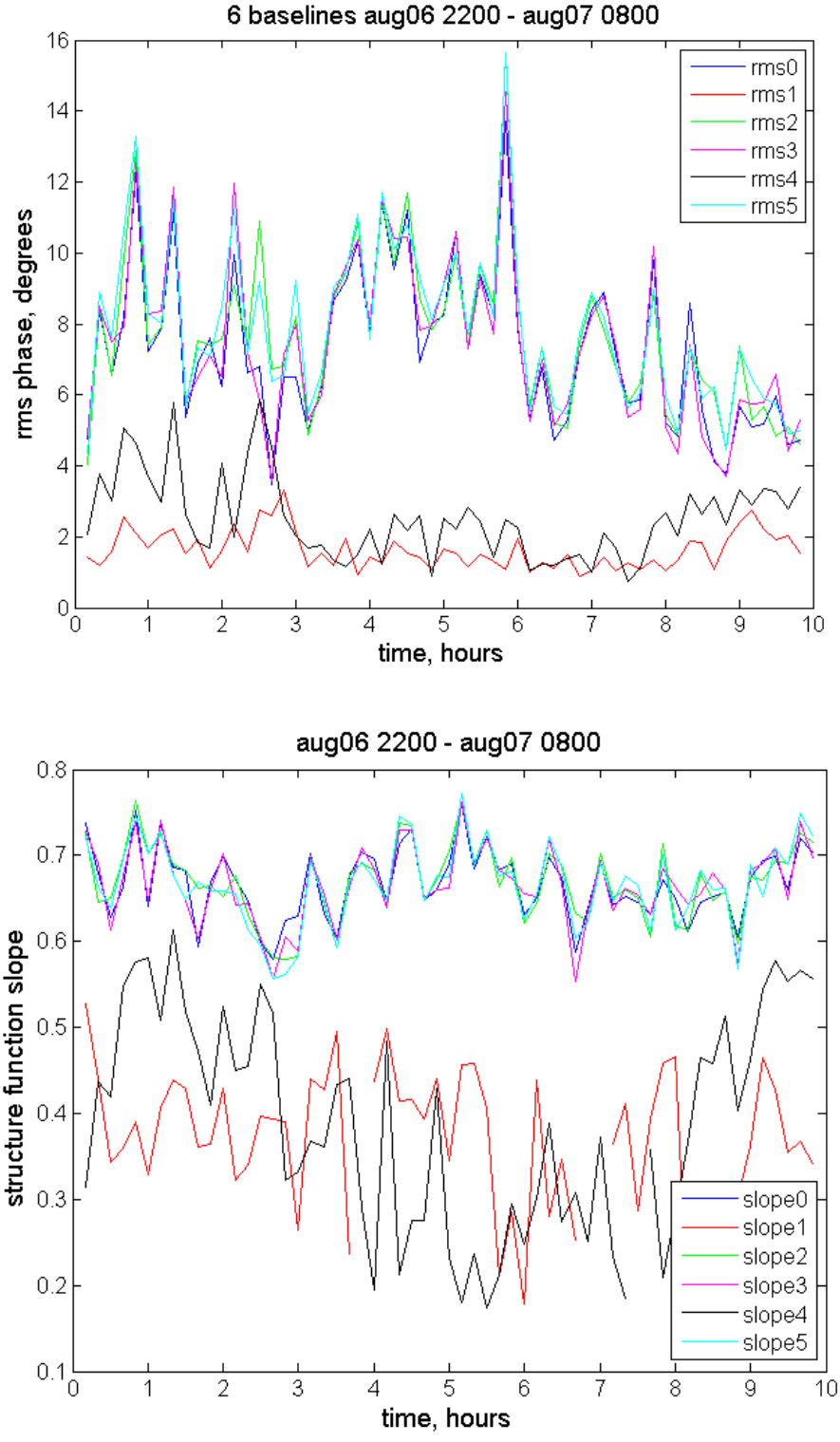


**Figure 17: RMS phase (above) and structure function slope (below) for the six API baselines for the night of Aug 6, 2014.**

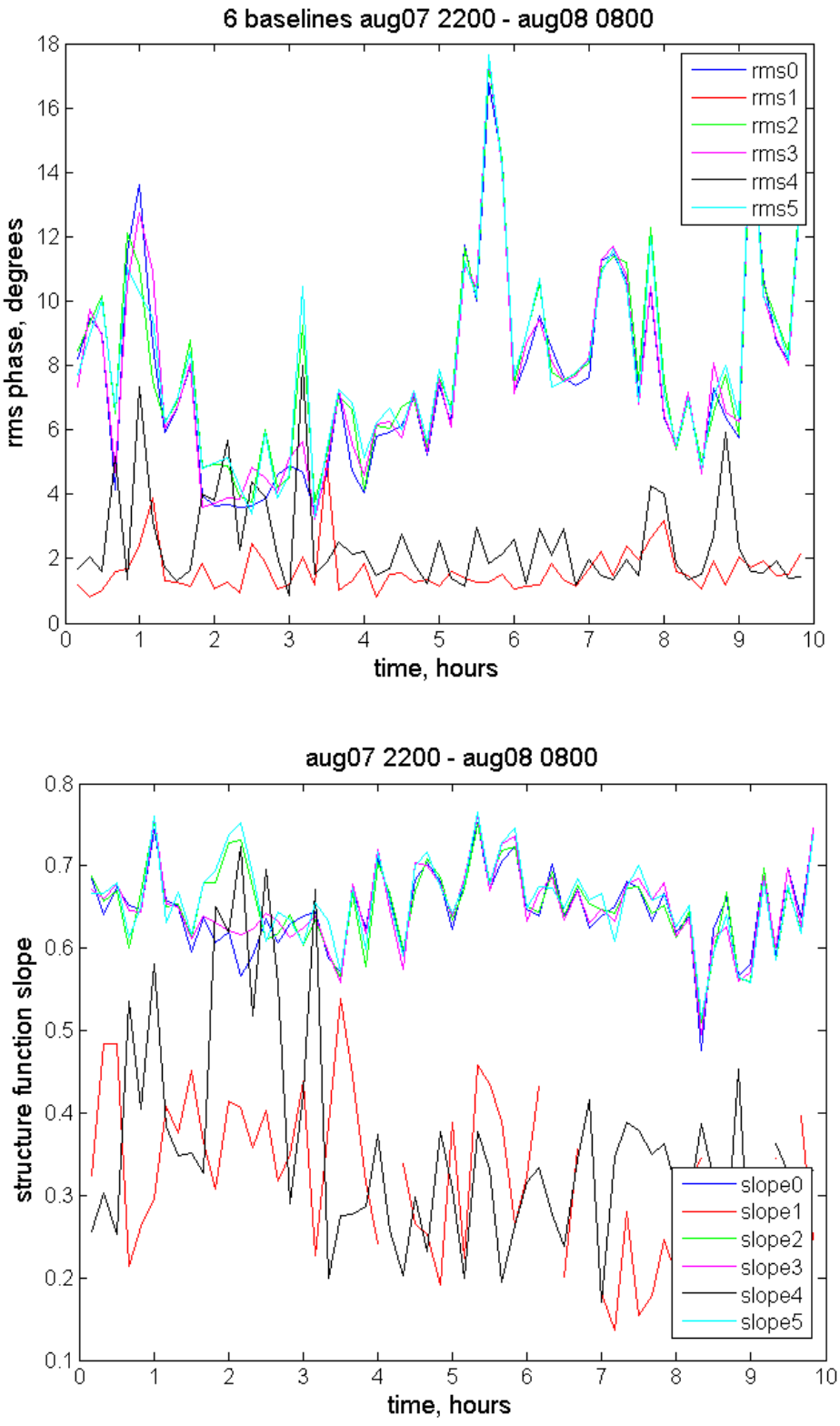


**Figure 18: RMS phase (above) and structure function slope (below) for the six API baselines for the night of Aug 7, 2014.**

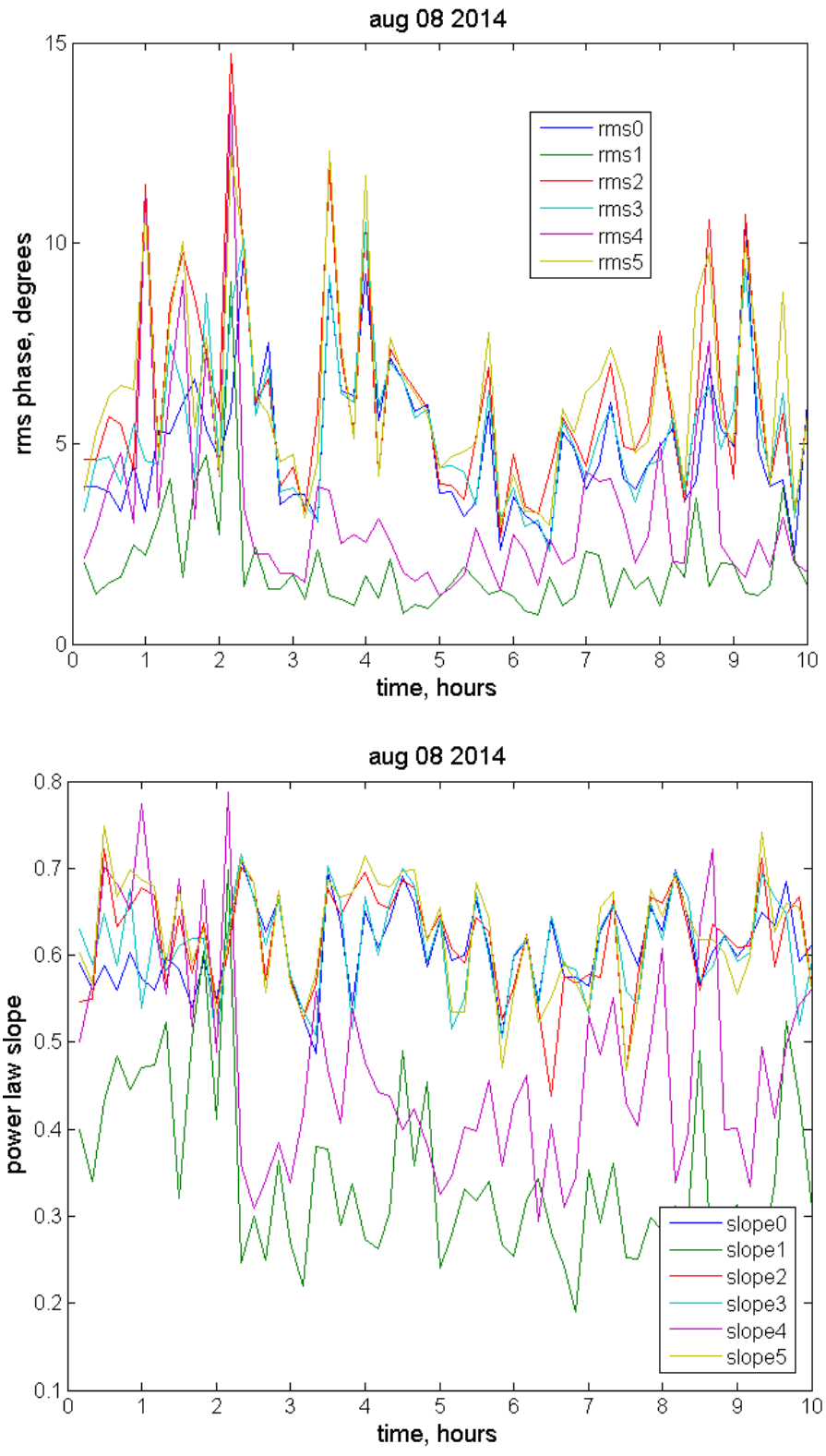


**Figure 19: RMS phase (above) and structure function slope (below) for the six baselines for the night of August 08, 2014.**

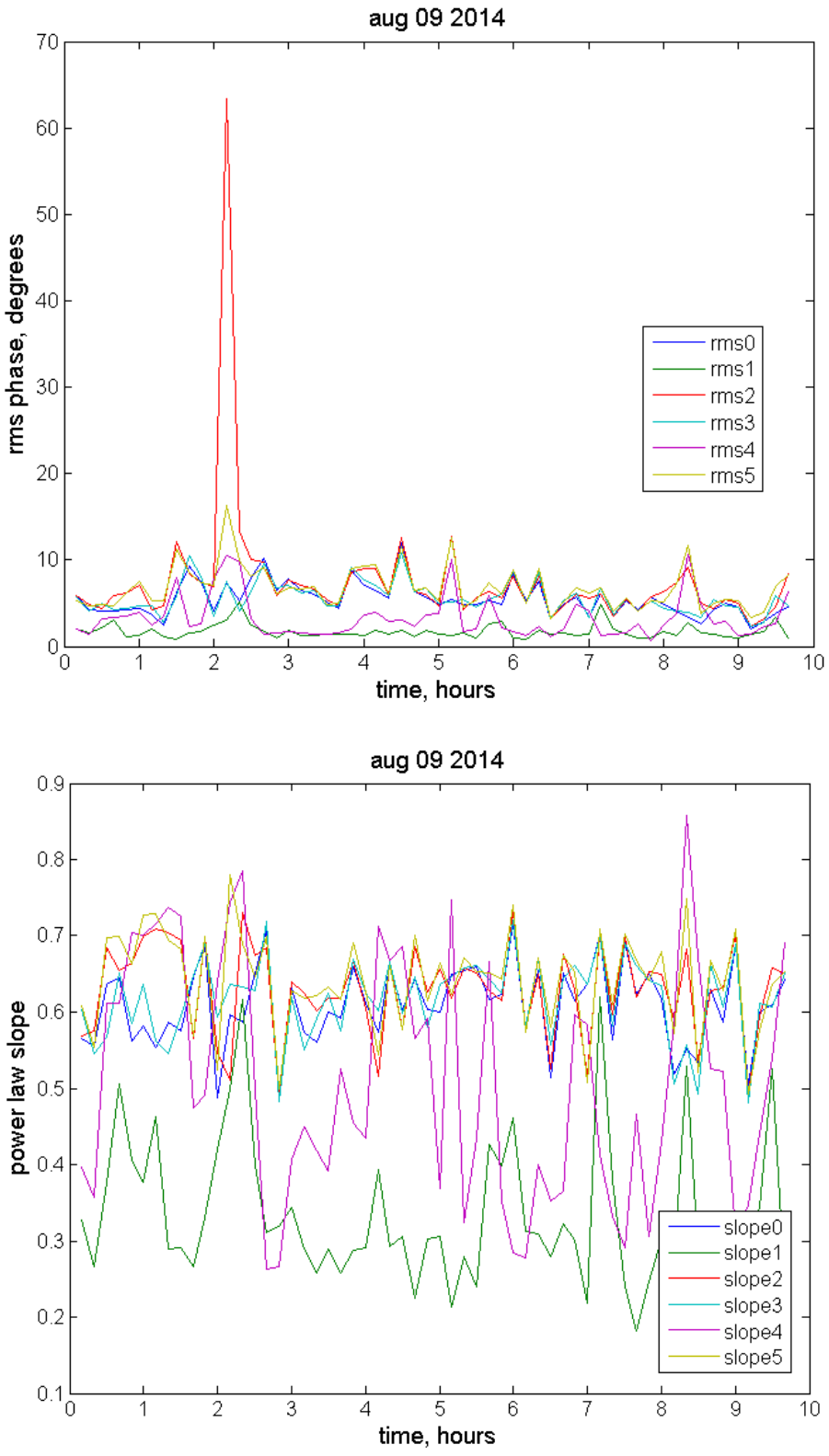


**Figure 20: RMS phase (above) and structure function slope (below) for the six baselines for the night of August 09, 2014**

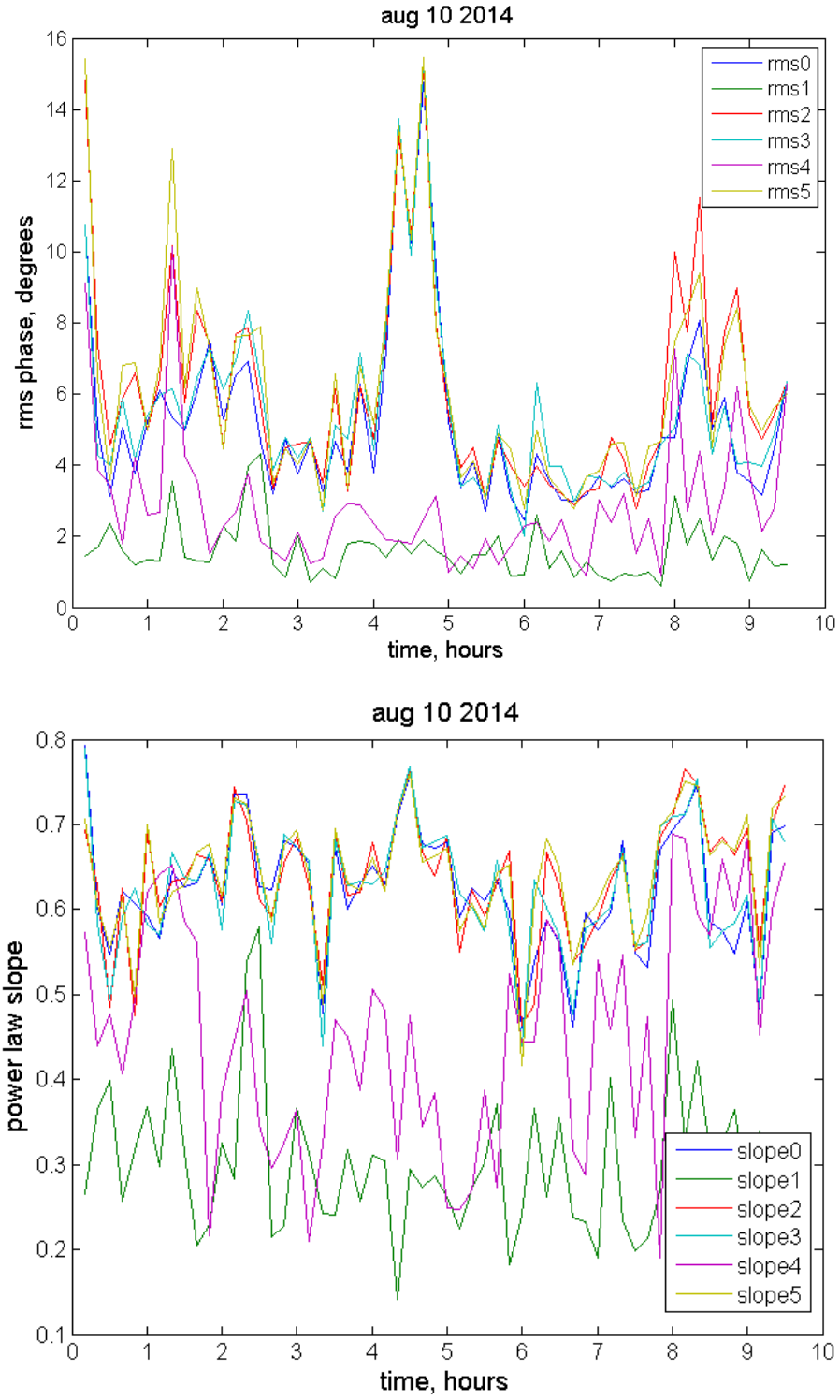


**Figure 21: RMS phase (above) and structure function slope (below) for the six baselines for the night of August 10, 2014.**